Dynamical Mountain Meteorology

Dr. Yuh-Lang Lin, ylin@cat.edu; http://mesolab.org
Department of Physics/Department of Energy & Environmental Systems
North Carolina A&T State University
(Ref.: *Mesoscale Dynamics*, Y.-L. Lin, Cambridge, 2007)

Chapter 8 Nonlinear Flow over Two-Dimensional Isolated Mountains

[Based on Sec. 5.3 of *Mesoscale Dynamics* (Lin 2007)]

5.3 Nonlinear Flow over Two-Dimensional Isolated Mountains

(Based on 5.3 Nonlinear flows over two-dimensional mountains – Lin 2007)

- As discussed in Sections 5.1 and 5.2, the response of a stably stratified flow over a two-dimensional mountain ridge has been studied extensively since the 1960's (e.g., Queney et al. 1960; Smith 1979).

- In particular, the linear dynamics are fundamentally understood, especially due to the development of linear theories in earlier times.

- Linear theory, however, begins to break down when the perturbation velocity (u') becomes large compared with the

basic flow (U) in some regions where the flow becomes stagnant.

- This may happen when the mountain becomes very high, the basic flow becomes very slow, or the stratification becomes very strong. In other words, flow becomes more nonlinear when the Froude number, $F = U / Nh$, becomes small. For simplicity, the mountain height is denoted by h.

- Thus, in order to fully understand the dynamics of nonlinear phenomena, such as upstream blocking, wave breaking, severe downslope winds and lee vortices, we need to take a nonlinear approach.

- Note that the reciprocal of the Froude number, Nh/U , has also been used as a control parameter and is known as *nondimensional mountain height*. The reason for using this terminology is that some meteorologists argue that U/Nh does not represent the ratio of kinetic energy and potential energy as originally defined for shallow-water fluid flow, $U/(gH)^{1/2}$.

  However, a recent study (Sun and Sun 2015, Geosci. Lett, 2:7; DOI 10.1186/s40562-015-0024-1) indicated that it does represent the same meaning. In the text, we will use these two parameters interchangeably.

- Nonlinear response of a continuously stratified flow over a mountain is very complicated since the nonlinearity may come from the basic flow characteristics, the mountain height, or the transient behavior of the internal flow, such as wave steepening.

- In this section, we will begin with the discussion of a nonlinear theory developed by Long (1953), then discuss the two-dimensional flow regimes for a continuously stratified flow over a two-dimensional mountain with the help of nonlinear numerical models, and the generation mechanisms of severe downslope winds and wave breaking.

5.3.1 Nonlinear flow regimes

- The governing equation for the finite-amplitude, steady state, two-dimensional, inviscid, continuously and stably stratified flow may be derived (Long 1953):

$$\nabla^2\delta + \frac{1}{e}\frac{de}{dz}\left[\frac{\partial\delta}{\partial z} - \frac{1}{2}(\nabla\delta)^2\right] + \frac{N^2}{U^2}\delta = 0 \quad , \qquad (5.3.1)$$

where $\delta(x,z) = z - z_o$ is the streamline deflection at (x,z) from its far upstream, undisturbed height z_o; U and N are the far upstream basic flow speed and Brunt-Vaisala frequency,

respectively, at height z_o, and $e = (1/2)\rho_o U^2$ is the kinetic energy of the upstream flow.

- In deriving (5.3.1), it has been assumed that there is no streamline deflection far upstream. In order to solve the above nonlinear equation, (5.3.1), we must specify e.

- Under the special situation $de/dz = 0$ and when the flow is Boussinesq, which assumes that ρ is approximately constant and $U(z)$ and $N(z)$ are effectively constant, (5.3.1) becomes a linear *Helmholtz equation*,

$$\nabla^2 \delta + l^2 \delta = 0, \tag{5.3.2}$$

where $l = N/U$ is the Scorer parameter of the basic flow far upstream.

- The nonlinear lower boundary condition for (5.3.2) is given by

$$\delta(x, z) = h(x) \quad \text{at } z = h(x), \tag{5.3.3}$$

where $h(x)$ is the height of the mountain surface.

In other words, the nonlinear lower boundary condition is applied on the mountain surface, instead of approximately

applied at $z = 0$ as in the linear lower boundary condition, such as (5.1.10).

- Equation (5.3.2) with the lower boundary condition (5.3.3) forms Long's model, in which the steady-state nonlinear flow is remarkably described by a linear differential equation with constant coefficients.

  In fact, (5.3.2) is exactly the same differential equation which applies to infinitesimal perturbations adopted in many linear theories and discussed earlier in this chapter.

- The appropriate upper boundary condition for a semi-infinite fluid, such as the atmosphere, is the radiation or boundedness condition, similar to (5.2.3) in the Fourier space for a uniform basic flow over an infinitesimal mountain.

- Following the procedure for treating linear flow over small-amplitude mountains, we make the Fourier transform of (5.3.2),

$$\hat{\delta}_{zz} + (l^2 - k^2)\hat{\delta} = 0 . \qquad (5.3.4)$$

The general solution for the above equation is

$$\hat{\delta} = \hat{\delta}(k,0)e^{imz} \quad \text{for } l > k \text{ and} \qquad (5.3.5a)$$

$$\hat{\delta} = \hat{\delta}(k,0)e^{-\lambda z} \quad \text{for } l < k , \qquad (5.3.5b)$$

where $m = \sqrt{l^2 - k^2}$, and $\lambda = \sqrt{k^2 - l^2}$.

Note that the upper radiation and boundedness conditions have been applied to (5.3.5a) and (5.3.5b), respectively, while the linear lower boundary condition has been applied at $z = 0$, instead of at $z = h(x)$.

The streamline deflection in the physical space can then be obtained by taking the inverse Fourier transform

$$\delta(x,z) = \mathrm{Re}\left[\int_0^l \hat{\delta}(k,0)e^{imz}e^{ikx}dk + \int_l^\infty \hat{\delta}(k,0)e^{-\lambda z}e^{ikx}dk\right], \qquad (5.3.6)$$

which may be obtained numerically, as with the Fast Fourier Transform numerical technique.

- Since we have assumed the fluid is incompressible, it allows us to define a streamfunction, ψ, such that

$$u = \frac{\partial \psi}{\partial z} \text{ and } w = -\frac{\partial \psi}{\partial x} .$$

The density perturbation is related to ψ ,

$$\rho = \rho_o\left(1 - \frac{N^2}{gU}\psi\right);$$

$$N^2 = -\frac{g}{\rho_o}\frac{\partial \rho}{\partial z},$$

(5.3.7)

It can be derived that Ψ equals to $U(z-\delta)$. The exact nonlinear lower boundary condition, (5.3.3), can be implemented using an iterative method (e.g., Laprise and Peltier 1989a).

- Figure 5.8 shows streamlines of analytical solutions for flow over a semi-circle obstacle for the nondimensional mountain heights $Nh/U = 0.5$, 1.0, 1.27, and 1.5.

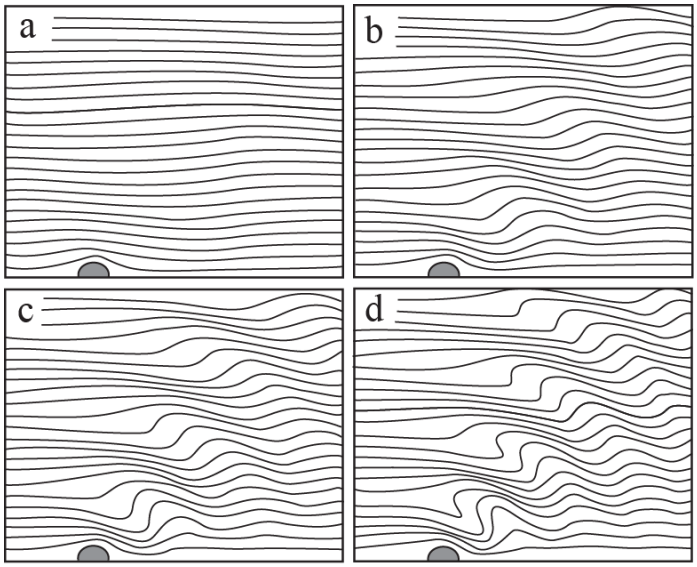

Fig. 5.8: Streamlines of Long's model solutions for uniform flow over a semi-circle obstacle with $Nh/U =$ (a) 0.5, (b) 1.0, (c) 1.27, and (d) 1.5, where Nh/U is the nondimensional mountain height or the reciprocal of the Froude number. Note that the streamlines become vertical in (c) and overturn in (d). (Adapted after Miles 1968)

- As mentioned earlier, the nondimensional mountain height is a measure of the nonlinearity of the continuously stratified flow, which equals the reciprocal of the Froude number (U/Nh).

When Nh/U is small, such as $Nh/U = 0.5$, the flow is more linear.

When Nh/U increases to 1.27, the flow becomes more nonlinear and its streamlines become vertical at the first level of wave steepening.

For flow with $Nh/U > 1.27$, the flow becomes statically and shear unstable (Laprise and Peltier 1989b). The vertical streamline marks the approximate limit of applicability of Long's model.

For the hydrostatic solution of Long's model with a bell-shaped mountain subject to a nonlinear lower boundary condition, this critical value is $Nh/U = 0.85$ (Miles and Huppert 1969) or $U/Nh = 1.18$.

Thus, for a continuously stratified, hydrostatic flow over a bell-shaped mountain, the flow may be classified as supercritical flow when $U/Nh > 1.18$ ($Nh/U < 0.85$) and as subcritical flow when $U/Nh < 1.18$ ($Nh/U > 0.85$).

Note that in the literature it is often misquoted $U/Nh = 1$ as the regime boundary for supercritical and subcritical regimes for continuously stratified flow over mountains.

- As discussed in Section 3.3, there exist five flow regimes in one-layer shallow-water system, based on the shallow water Froude number, $F = U/\sqrt{gH}$, and the nondimensional mountain height, $M = h_m / H$ (Fig. 3.3).

- In a non-rotating, continuously stratified flow over a two-dimensional, bell-shaped mountain, three nondimensional control parameters may be identified: U/Nh, h/a, and Na/U, based on Buckingham-Π theorem. However, only two of them are independent.

  U/Nh: Froude number or inverse nondimensional height

  h/a: Steepness of mountain

  Na/U: Nondimensional mountain width which measures the degree of hydrostatic effect (the larger the more hydrostatic).

  In the hydrostatic limit ($Na/U \to \infty$), the sole control parameter is the Froude number.

- Figure 5.9a shows streamlines for Long's solutions for flow over a bell-shaped mountain with a half-width (a) of 3 km with the nonlinear lower boundary condition (5.3.3) applied.

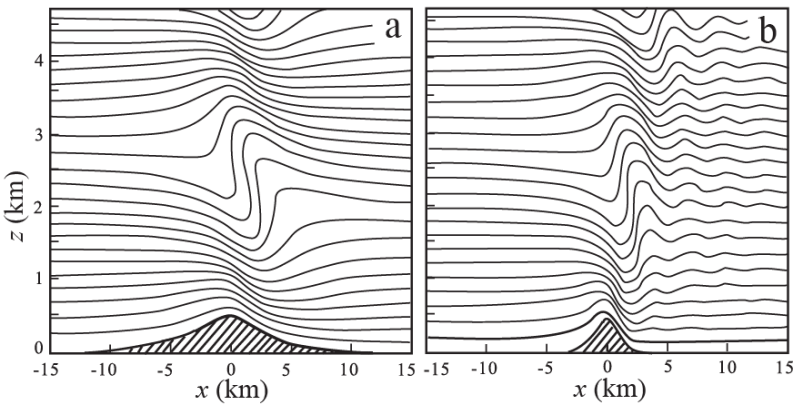

Fig. 5.9: (a) Streamlines for Long's model solution over a bell-shaped mountain with $U = 5$ ms^{-1}, N = 0.01 s^{-1}, $h_m = 500$ m and $a = 3$ km; and (b) same as (a) except with $a = 1$ km. An iterative method is adopted in solving the nonlinear equation (5.3.2) with the nonlinear lower boundary condition (5.3.3) applied. Note that the dispersive tail of the nonhydrostatic waves is present in the narrower mountain (case (b)). (Adapted from Laprise and Peltier 1989a)

Internal waves tend to overturn in regions of reversed density gradient (statically unstable), $\partial\rho / \partial z > 0$, which corresponds to $\partial\delta / \partial z > 1$ from (5.3.7). The heights of critical steepening levels differ slightly from those predicted by linear theory for hydrostatic waves, $z_o = (n + 3/4)(2\pi U / N)$, where n is an integer, just over the crest of the topography (Laprise and Peltier 1989a).

In Fig. 5.9a, the first steepening level for nonlinear, hydrostatic waves is about 2.36 km. With a narrower mountain, such as a = 1 km (Fig. 5.9b), a dispersive tail, caused by nonhydrostatic dispersion, is produced.

The downstream displacement of the steepened region is caused by both the nonhydrostatic effect and the nonlinearity of the interior flow and the lower boundary condition.

When $Na/U >> 1$, the flow approaches the hydrostatic limit. This control parameter can be obtained by comparing the scales of $\partial^2 w'/\partial x^2$ and $N^2 w'/U^2$ of (5.1.5).

$$\nabla^2 w' + l^2(z) w' = 0 .$$

Direct comparison of $\partial^2 w'/\partial x^2$ and $\partial^2 w'/\partial z^2$ terms by scale analysis leads to the conclusion that *h/a* is a control parameter of nonhydrostatic effect.

The Froude number, U/Nh, can also be derived by comparing the scales of $\partial^2 w'/\partial z^2$ and $N^2 w'/U^2$ of (5.1.5).

Remember, in Sec. 5.1, we have discussed about

It may also be interpreted as a vorticity equation upon being multiplied by U (Smith 1979).

The first term, $U(w'_{xx} + w'_{zz})$, is the rate of change of vorticity following a fluid particle.

The second term, $N^2 w'/U$, is the rate of vorticity production by buoyancy forces.

- Long's nonlinear theory advances our understanding of orographically forced flow considerably. However, the constant upstream condition assumed by Long may not be necessarily consistent with the flow established naturally by transients, especially when blocking occurs (Garner, 1995).

- In the real atmosphere, turbulence will come into play and produce vertical mixing in a subcritical (overturning) flow. To simulate a subcritical flow, one may consider using a laboratory tank experiment or adopting a nonlinear numerical model.

- As mentioned earlier, flow may become stagnant, where the total horizontal wind speed reduces to zero ($u = U + u' = 0$), in essentially two regions: in the interior of the fluid over the mountaintop or on the lee slope and along the upstream slope of the mountain.

- *Flow stagnation* in a two-dimensional flow is responsible for *flow recirculation*, while stagnation in a three-dimensional flow is responsible for *flow splitting*.

  Flow stagnation in the interior of the fluid is due to nonlinear *wave steepening*, which may lead to *wave breaking* and *wave overturning* over the lee slope, while the flow stagnation at the upstream surface of the mountain is called *flow blocking*.

- Although the two-dimensional, nonrotating, hydrostatic flow may be simply classified as supercritical and subcritical regimes, as discussed above, the transient flow behavior becomes much more complicated.

- Figure 5.10 shows the time evolution for the θ and u' fields for a hydrostatic flow over a two-dimensional, bell-shaped mountain simulated by a numerical model at nondimensional times $Ut/a = 12.6$ and 50.4 for F ranging from 0.5 to 1.3.

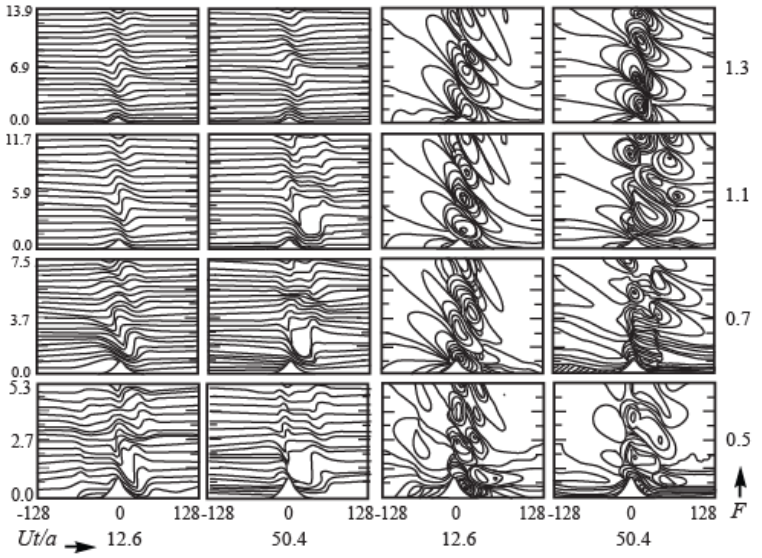

Fig. 5.10: Nonlinear flow regimes for a two-dimensional, hydrostatic, uniform flow over a bell-shaped mountain as simulated by a numerical model, based on the Froude number ($F = U/Nh$). F varies from 0.5 to 1.3, which gives four different flow regimes as discussed in the text. Displayed are the θ fields (left two columns) and the u' fields (right two columns) for two nondimensional times $Ut/a = 12.6$ and 50.4. The dimensional parameters are: $N = 0.01$ ms^{-1}, h = 1 km, a = 10 km, and U = 5, 7, 11, and 13 ms^{-1} corresponding to F = 0.5, 0.7, 1.1, and 1.3, respectively. A constant nondimensional physical domain height of $1.7\lambda_z$ (where $\lambda_z = 2\pi U/N$) is used. Both the abscissa and ordinate in the small panels are labeled in km. (Adapted after Lin and Wang 1996)

- Four regimes are identified:
  (I) flow with neither wave breaking aloft nor upstream blocking (e.g., $1.12 \le F$)
  (II) flow with wave breaking aloft in the absence of upstream blocking (e.g., $0.9 \le F < 1.12$)
  (III) flow with both wave breaking and upstream blocking, but where wave breaking occurs first (e.g., $0.6 \le F < 0.9$)
  (IV) flow with both wave breaking and upstream blocking, but where blocking occurs first (e.g., $0.3 \le F < 0.6$).

- Note that the exact Froude numbers separating these flow regimes might be different in other numerically simulated results because these numbers are sensitive to some numerical factors, such as the grid resolution, domain size, numerical boundary conditions, and numerical scheme adopted in different numerical models.

- Regime I (e.g., $F = 1.3$ in Fig. 5.10), neither wave breaking nor upstream blocking occurs, but an upstream propagating *columnar disturbance* does exist. The basic flow structure in regime I resembles linear mountain waves.

  Columnar disturbances are wave modes with constant phase in the vertical, which permanently alter the upstream temperature and horizontal velocity fields as they pass through the fluid (e.g., Pierrehumbert and Wyman 1985). A columnar disturbance may be generated by a sudden

imposition of a disturbance, such as the impulsive introduction of a mountain in a uniform flow.

- Regime II (e.g., $F = 1.1$ in Fig. 5.10) resembles weakly nonlinear mountain waves: flow with wave breaking aloft in the absence of upstream blocking (e.g., $0.9 \le F < 1.12$).

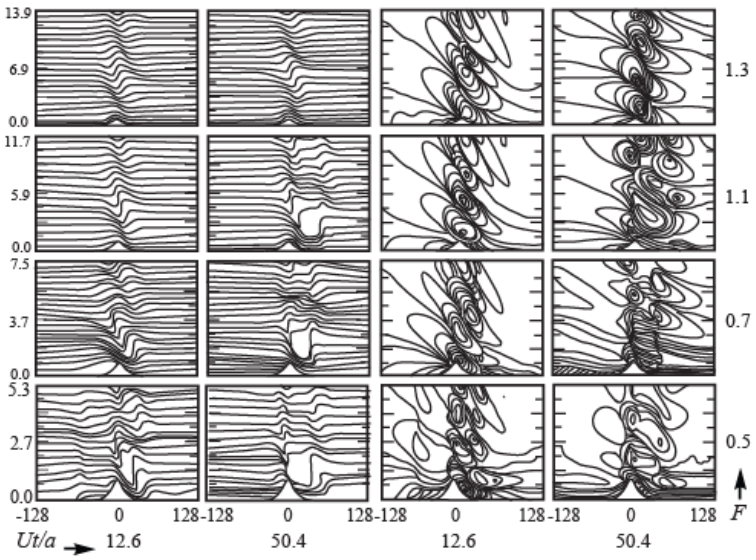

In this flow regime, an internal jump forms at the downstream edge of the wave-breaking region above the mountain, propagates downstream, and then becomes quasi-stationary. The region of wave breaking also extends downward toward the lee slope.

After the internal jump travels farther downstream, a stationary mountain wave becomes established in the vicinity of the mountain above the dividing streamline, which is induced by wave breaking.

A high-drag state is predicted in this flow regime. In addition, a vertically propagating hydrostatic gravity wave is generated by the propagating jump and travels with it.

Along the lee slope, a strong downslope wind develops. Static and shear instabilities may occur locally in the region of wave breaking. The computed critical Froude number for wave breaking is about 1.12, which agrees well with the value 1.18 found by Miles and Huppert (1969).

- Regime III: flow with both wave breaking and upstream blocking, but where wave breaking occurs first (e.g., $0.6 \le F < 0.9$).

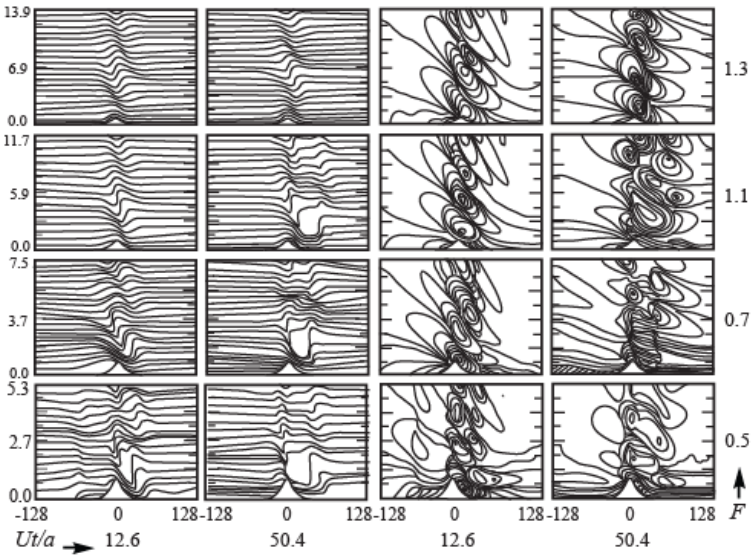

In regime III (e.g., $F = 0.7$ in Fig. 5.10), the internal jump over the lee slope propagates downstream in the early stage and then becomes quasi-stationary.

Note that the propagation of the downstream internal jump is sensitive to the upstream numerical boundary condition, which may cause the internal jump to retrogress upstream. To avoid this artificial effect from the numerical model, the upstream boundary should be placed far enough so as to effectively reduce its impact.

Also, the layer depth of blocked fluid upstream is independent of the Froude number.

- Regime IV: flow with both wave breaking and upstream blocking, but where blocking occurs first (e.g., $0.3 \le F < 0.6$).

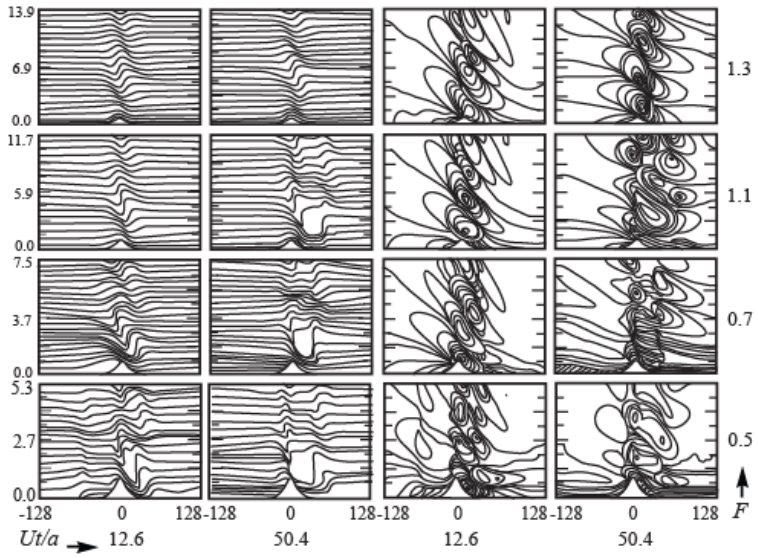

Fig. 5.10

In regime IV (e.g., $F = 0.5$ in Fig. 5.10), a significant portion of the upstream flow is blocked by the mountain.

The presence of wave breaking aloft is not a necessary condition for upstream blocking to occur.

A vertically propagating gravity wave is generated by the upstream reversed flow and travels with it. The speed of the upstream reversed flow is proportional to h/a. The surface drag increases abruptly from regime I to II, while it decreases gradually from regime II (III) to III (IV).

- Note that flow regimes may also be classified in different ways, depending upon particular characteristics. For example, two-dimensional, uniform flow over an isolated mountain has been classified as either a quasi-linear regime, high-drag state, or blocked state, based on Nh/U and NU/g (Stein 1992).

In addition, the flow response of a three-dimensional flow over a long ridge is very different from that of a two-dimensional flow when Nh/U is large. For example, the onset of wave breaking and the transition to the high-drag state in the three-dimensional flow was found to be accompanied by an abrupt increase in deflection of the low-level flow around the ridge (Epifanio and Durran 2001). The increased flow deflection is produced at least in part by upstream-propagating columnar disturbances forced by the transition to the high-drag state.

5.3.2 Generation of severe downslope winds

- Severe downslope winds over the lee of a mountain ridge have been observed in various places around the world, such as the

  Chinook over the Rocky Mountains,
  Santa Ana winds in southern California, and
  Diabolo winds in San Francisco Bay Area.
  Foehn over the Alps,
  Bora over the Dinaric Alps,
  Zonda over the Agentina mountains,
  Berg wind in South Africa,
  Canterbury-nor'wester in New Zealand,
  Halny wiatr in the mountains of Poland.

  One well-known event is the 11 January 1972 windstorm which occurred in Boulder, Colorado, and which reached a peak wind gust as high as 60 ms^{-1} and produced severe damage in the Boulder area (Fig. 3.4a).

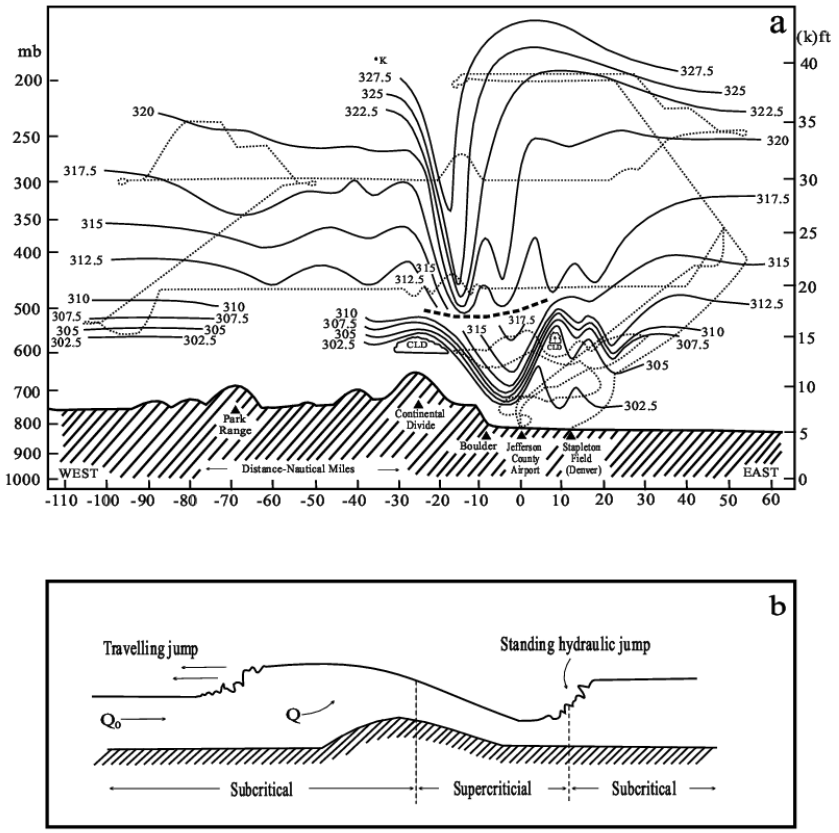

Fig. 3.4: (a) Analysis of potential temperature from aircraft flight data and rawinsondes for the 11 January 1972 Boulder *windstorm*. Aircraft tracks are shown by dashed lines with locations of significant turbulence shown by plus signs. The heavy dashed line separates data taken by the Queen Air aircraft (before 2200 UTC) and from the Saberliner aircraft (after 0000 UTC) (Adapted after Klemp and Lilly 1975). The severe downslope wind reached a value greater than 60 ms^{-1}. (b) A sketch of flow Regime c of Fig. 4.3, which may be used to explain the phenomenon associated with (a). Q represents the volume flux per unit width. (Lin 2007; Adapted after Turner 1973)

- The basic dynamics of the severe downslope wind can be understood from the following major theories:
  (a) *Resonant amplification theory* (Clark and Peltier 1984, Wang and Lin 1999, Xeiteira et al. 2005)

(b) *Hydraulic theory* (Smith 1985, Durran and Klemp 1987, Bacmeister and Pierrehumbert 1988, Rottman and Smith 1989,Wang and Lin 2005)

The above theories will be reviewed in the following. Also see Lin (2007) for detailed review and discussion.

a. Resonant amplification theory

- Idealized nonlinear numerical experiments indicate that a high-drag (severe-wind) state occurs after an upward propagating mountain wave breaks above a mountain, such as happens in Fig. 5.10 ($F = 0.5$, 0.7, and 1.1), in which severe downslope winds develop in a uniform flow over a bell-shaped mountain. The wave-breaking region is characterized by strong turbulent mixing (where $Ri < 0.25$), with a local wind reversal on top of it.

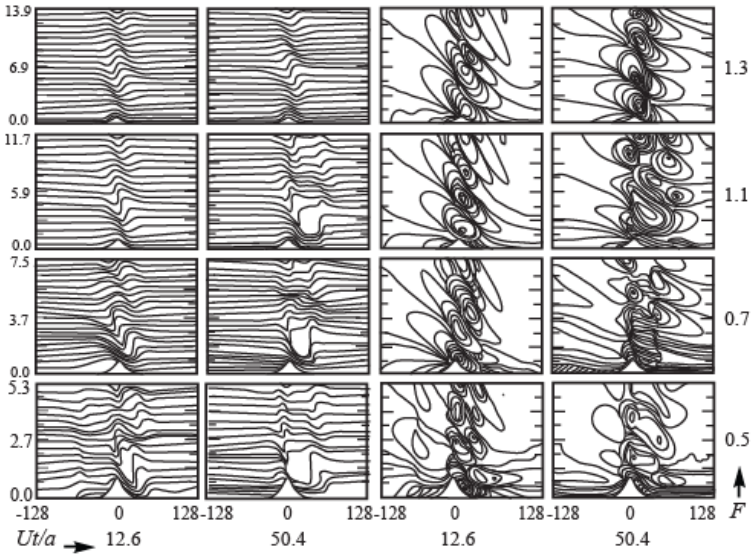

Fig. 5.10

- As mentioned in Section 3.8, the *wind reversal level* coincides with the critical level for a stationary mountain wave, and thus is also referred to as the *wave-induced critical level*. The lowest wave-induced critical level starts to develop at the height $z = 3\lambda_z / 4 \approx 2.36$, 3.30, and 5.18 km for cases of $F =$ 0.5, 0.7, and 1.1, respectively (at $Ut / a = 12.6$ in Fig. 5.10), where λ_z $(= 2\pi U / N)$ is the hydrostatic vertical wavelength.

  A supercritical flow with a severe downslope wind can be found over the lee slope under the wave breaking region, which undergoes a transition from subcritical flow over the upwind slope.

- The maximum perturbation wind over the lee slope is much higher than those predicted by linear and weakly nonlinear theories. At a later stage, the *well-mixed layer* (*wake*) deepens, the depth of *internal hydraulic jump* (critically steepened streamlines) extends to a great depth, the flow above the initial wave-induced critical level is less disturbed compared to that in the lower layer, and severe winds develop over the lee slope and below the well-mixed layer ($Ut / a = 50.4$ in Fig. 5.10).

- The above example implies that the wave breaking region aloft acts as an internal boundary which reflects the upward propagating waves back to the ground and produces a high-

drag state through partial resonance with the upward propagating mountain waves. This is shown by performing nonlinear numerical simulations for stratified flow over a bell-shaped mountain (Fig. 5.11).

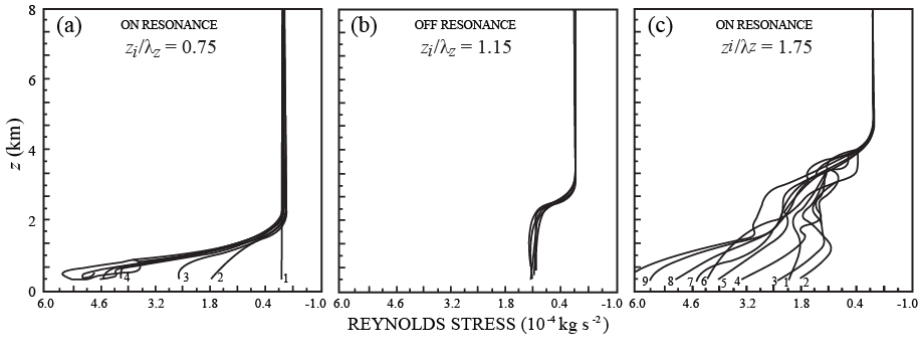

Fig. 5.11: Resonant amplification mechanism for severe downslope winds developed for basic flow with a prescribed critical level (z_i) over a bell-shaped mountain. Displayed are the evolution of the Reynolds stress, $\langle \rho_o u' w' \rangle$, profile for on-resonance flows with: $z_i / \lambda_z =$: (a) 0.75 and (c) 1.75 and for the off-resonance flow with (b) $z_i / \lambda_z = 1.15$, where $\lambda_z = 2\pi U_o / N$. The flow and orographic parameters are: $N = 0.02\, s^{-1}$, $U(z) = U_o \tanh[(z - z_i)/b]$ with $U_o = 8$ ms^{-1}, $b = 600$ m, $Ri_{\min} = N^2/(U_o/b)^2 = 2.25$ (minimum Ri), $h = 300$ m, and $a = 3$ km. The Froude number (U_o / Nh) is 1.33. Height (z) is in km. The profiles in the figure range in time from 0 to 2880 Δt, 1440 to 2880 Δt, and 2080 to 4240 Δt for panels (a) to (c), respectively, where $\Delta t = 5$ s. Some of the profiles are sequentially numbered from earliest to latest (labeled by small numbers). (Lin 2007; After Clark and Peltier 1984)

In these simulations, the basic flow reverses its direction at a prescribed critical level (z_i). In the absence of shear instability associated with the basic flow, and when the basic-flow critical level is located at a nondimensional height of $z_i/\lambda_z = 3/4 + n$ (n is an integer) above the surface, nonlinear resonant amplification occurs between the upward propagating waves generated by the mountain and the downward propagating waves reflected from the critical level.

This leads to an extremely large Reynolds stress or surface drag and severe downslope winds (Figs. 5.11a and 5.11c). In other words, the flow is *on resonance*.

On the other hand, when the basic flow critical level is located at a nondimensional height off $z_i/\lambda_z = 3/4 + n$, such as 1.15, there is no wave resonance and no severe downslope winds generated (Fig. 5.11b).

Because the severe downslope winds are developed by resonance between upward and downward waves, this mechanism is referred to as the *resonant amplification mechanism*.

Based on numerical simulations with finer-grid resolutions, Scinocca and Peltier (1993) proposed three distinct stages for the development of severe downslope winds:

(1) Local static (buoyancy) instability develops when the wave steepens and overturns, thus producing a pool of well-mixed air aloft (Figs. 5.12a-b).

(2) A well-defined large-amplitude stationary disturbance is generated over the lee slope. In time, small-scale secondary Kelvin-Helmholtz (K-H) (shear) instability

develops in local regions of enhanced shear associated with flow perturbations caused by the large-amplitude disturbance (Figs. 5.12c-d).

(3) The region of enhanced wind on the lee slope expands downstream, eliminating the perturbative structure associated with the large-amplitude stationary disturbance (Figs. 5.12e-f).

The K-H instability dominates the flow in this mature windstorm state. Thus, static instability helps explain the initiation of wave-induced critical level and the downstream expansion of the severe downslope winds.

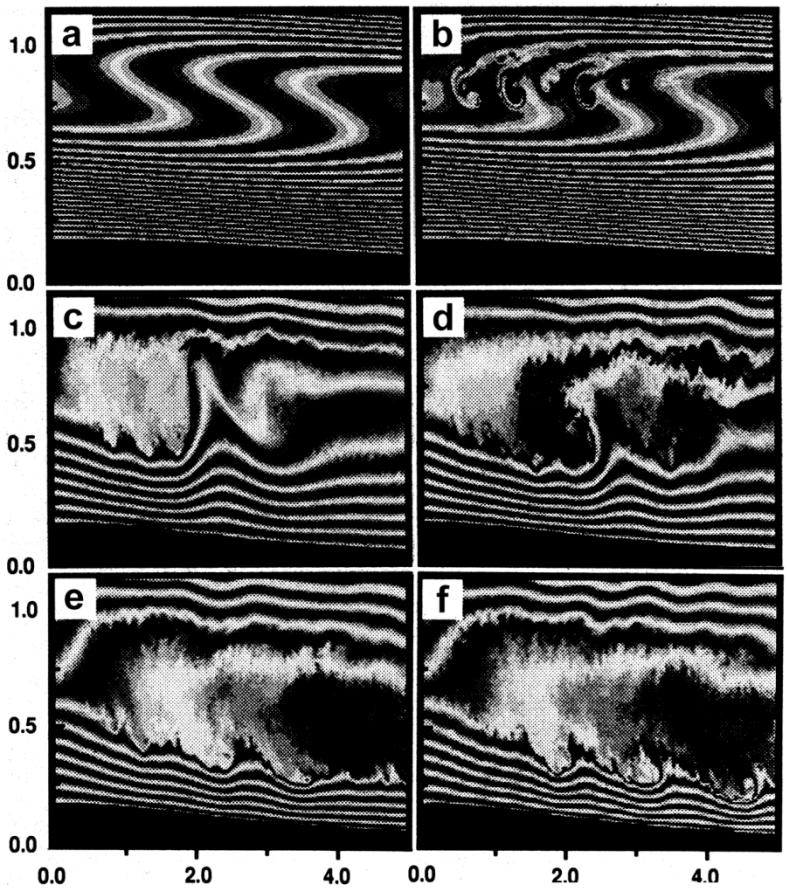

Fig. 5.12: Three distinct stages for the development of severe downslope winds, as revealed by the triply-nested numerical simulations (see text for details). Long's (1953) nonlinear analytical solution is used to initiate the flow. Displayed are the potential temperature fields over the lee slope at model times of (a) 0, (b) 20, (c) 66, (d) 96, (e) 160, and (f) 166 min. The grid resolutions for the outer, middle, and inner domains are 500 m, 50 m, and $16\frac{2}{3}$ m, respectively. A bell-shaped mountain with h = 165 m and a = 3 km is used. The upstream flow parameters are U = 3.3 ms^{-1} and N = 0.02 s^{-1}. Thus, $F = U/Nh = 1$. (Lin 2007; Adapted after Scinocca and Peltier 1993)

Once wave breaking occurs, it induces a critical level in the shear layer with low *Ri* and thus establishes a flow configuration favorable for *wave ducting* in the lower uniform flow layer, similar to that in case 3 of Table 4.1 and Fig. 4.12b.

- Effects of the wave ducting on the development of high-drag states for a flow with uniform wind and constant static stability are illustrated in Fig. 5.13 (Wang and Lin 1999; reviewed in Lin 2007).

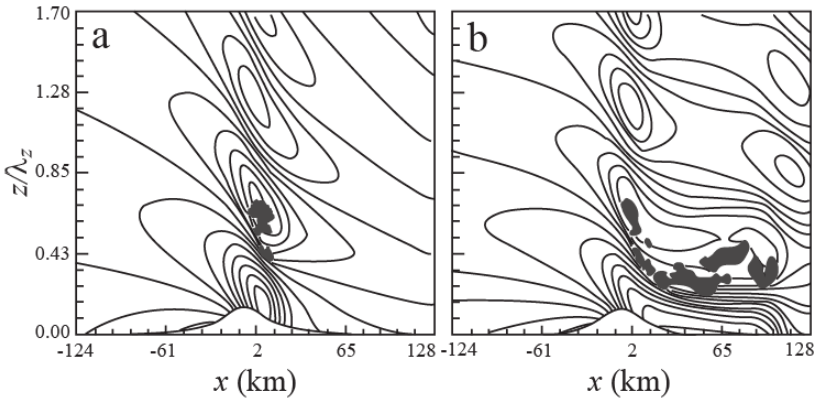

Fig. 5.13: Wave ducting as revealed by the time evolution of horizontal wind speeds and regions of local $Ri < 0.25$ (shaded) for a flow with uniform wind and constant static stability over a mountain ridge at $Ut/a =$ (a) 12.6, and (d) 50.4. The Froude number of the uniform basic wind is 1.0. (Lin 2007; Adapted after Wang and Lin 1999)

Shortly after the occurrence of wave breaking, regions with local $Ri < 0.25$ form in the vicinity of the wave breaking (Fig. 5.13a).

This turbulent mixing region is expanding downward and downstream due to strong nonlinear effects on the flow with low Richardson number near the critical level (Fig. 5.14a).

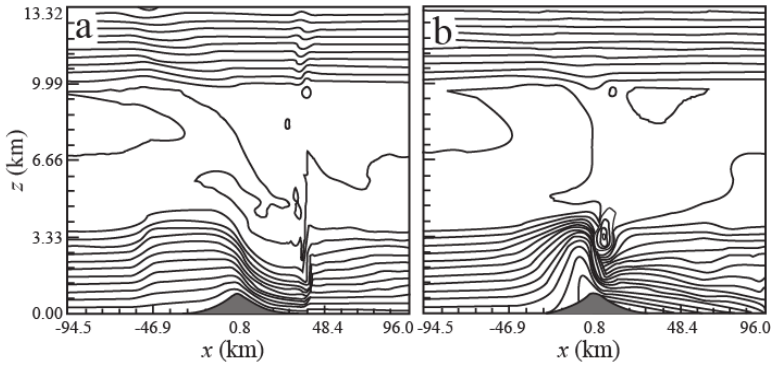

Fig. 5.14: Effects of nonlinearity on the development of severe downslope winds: (a) Potential temperature field from nonlinear numerical simulations for a basic flow with $Ri = 0.1$ and $F = 2$; (b) Same as (a) except from linear numerical simulations. The contour interval is 1 K in both (a) and (b). (Lin 2007; Adapted after Wang and Lin 1999)

The turbulent mixing region expands downward by wave reflection, overreflection, and ducting from the wave-induced critical level and accelerates downstream by the nonlinear advection (Fig. 5.13b of Wang and Lin 1999).

Effects of wave reflection and/or overreflection are evidenced by the fact that the wave duct with severe downslope wind is located below the region of the turbulent mixing region.

Note that the expansion of the turbulent mixing region provides a maintenance mechanism for the existence of the wave duct below it and above the lee slope, because the reflectivity in this region is about 1, according to linear theory (Wang and Lin 1999; Lin 2007).

Without this almost perfect reflector, the wave below cannot be maintained and would lose most of its energy due to dispersion. In fact, wave overreflection can occur, according to the wave ducting theory discussed in Chapter 4, through the extraction energy from the well-mixed region and thus contribute to the acceleration of downslope winds.

In the absence of nonlinearity (Fig. 5.14b), the wavebreaking region does not expand downward to reduce the depth of the lower uniform wind layer. This, in turn, prohibits the formation of the severe downslope wind and internal hydraulic jump. These results indicate that the nonlinear wave ducting has contributed to the downward and downstream expansion of the turbulent mixing region.

- ***Hydraulic theory***

Based on the similarity of flow configurations of severe downslope windstorms and finite-depth, homogeneous flow over a mountain ridge, a nonlinear hydraulic theory was proposed to explain the development of severe downslope winds (Smith 1985).

The hydraulic theory attributes the high-drag (severe-wind) state to the interaction between a smoothly stratified flow and the deep, well-mixed, turbulent "dead" region above the lee slope in the middle troposphere. When a high-drag state

develops, a *dividing streamline* encompasses this well-mixed region of uniform density (ρ_c in Fig. 5.15a).

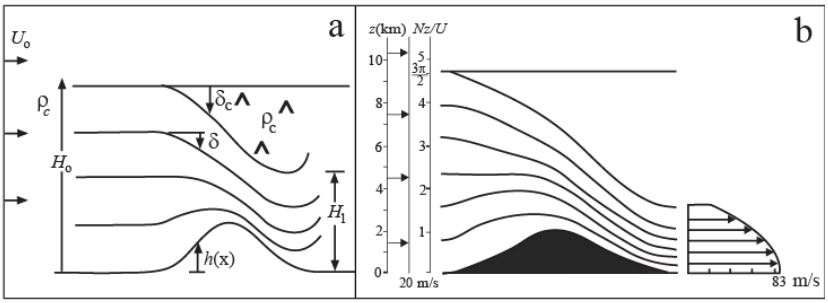

Fig. 5.15: A severe downslope windstorm simulated by a hydraulic theory. (a) Schematic of an idealized high-drag state flow configuration. A certain critical streamline divides and encompasses a region of uniform density (ρ_c), which is called dividing streamline. H_o and H_1 denote the heights of upstream dividing streamline and downstream lower dividing streamline, respectively. (b) An example of transitional flow over a mountain. The dimensional values of the flow and orographic parameters are $U = 20$ ms^{-1}, $N = 0.01$ s^{-1}, $H_o = 9.42$ km, and $h = 2$ km. This gives $F = U/Nh = 1.0$. (Lin 2007; Adapted after Smith 1985)

Assuming the upstream flow is uniform in U and N and the general flow is smooth, nondissipative, hydrostatic, Boussinesq and steady (Fig. 5.15a), the nonlinear, hydrostatic governing equation can be simplified from (5.3.1),

$$\delta_{zz} + l^2\delta = 0\,, \tag{5.3.8}$$

The horizontal velocity can be derived from (5.3.7),

$$u = U(1 - \delta_z)\,. \tag{5.3.9}$$

The lower boundary condition is given by (5.3.3).

$$\delta(x,z) = h(x) \quad \text{at } z = h(x), \tag{5.3.3}$$

By assuming no disturbance above the upper dividing streamline (H_o), the pressure at $z = H_o$ is constant, i.e $p(x,H_o) = p^*$.

If the air in the turbulent region is hydrostatic in the mean and well mixed with a density of ρ_c, the pressure along the lower branch of the dividing streamline is $p(x,H_o + \delta_c) = p^* - \rho_c g \delta_c$, where δ_c is the vertical displacement of the lower dividing streamline (H_1).

For a steady-state flow, the Bernoulli equation along $z = H_o + \delta_c$ can be written

$$p + (1/2)\rho u^2 + \rho_c g z = constant. \tag{5.3.10}$$

At $z = H_o + \delta_c$, we have

$$\delta_z = 0. \tag{5.3.11}$$

By assuming a wave-like solution in the vertical,

$$\delta(x,z) = A(x)\cos lz + B(x)\sin lz\,, \qquad (5.3.12)$$

the nonlinear solution for high-drag state can be obtained,

$$\tilde{h} = \tilde{\delta}_c[\cos(\tilde{H}_o + \tilde{\delta}_c - \tilde{h})], \qquad (5.3.13a)$$

$$\tilde{A} = \tilde{\delta}_c \cos(\tilde{H}_o + \tilde{\delta}_c)\,, \text{ and} \qquad (5.3.13b)$$

$$\tilde{B} = \tilde{\delta}_c \sin(\tilde{H}_o + \tilde{\delta}_c)\,, \qquad (5.3.13c)$$

where $h(x)$ is the terrain height function and all coefficients and parameters are nondimensionalized by l (= N/U) and denoted by tilde's ("~"). The above solution can be solved graphically or numerically as long as $\tilde{h}$ and $\tilde{H}_o$ are known.

Figure 5.15 shows an example of a severe downslope windstorm simulated by a hydraulic theory with $F = 1.0$.

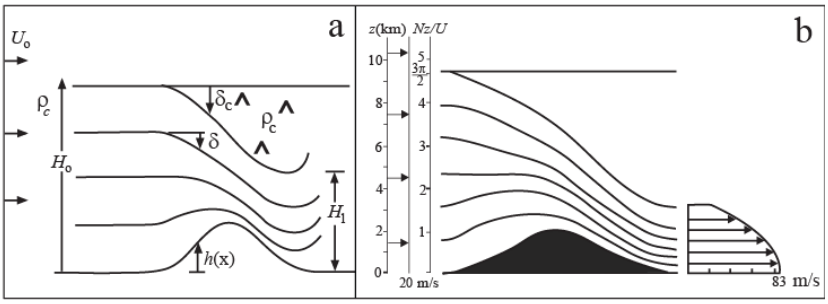

Fig. 5.15

The descent of the lower dividing streamline begins over the point where the mountain begins to rise and becomes more rapid over the mountain peak.

The final downward displacement of the dividing streamline is a large fraction of the initial layer depth. The flow speed after transition to supercritical flow over the lee slope from subcritical flow over the upslope is greatest near the surface and is several times the upstream value. The flow shown in Fig. 5.15b is qualitatively similar to the 1972 Boulder windstorm observations (Fig. 3.4a).

In addition to the above solution, the strength of the transitional flow can be measured by the pressure drag on the mountain per unit length,

$$D = \frac{\rho_o N^2}{6}(H_o - H_1)^3 . \qquad (5.3.14)$$

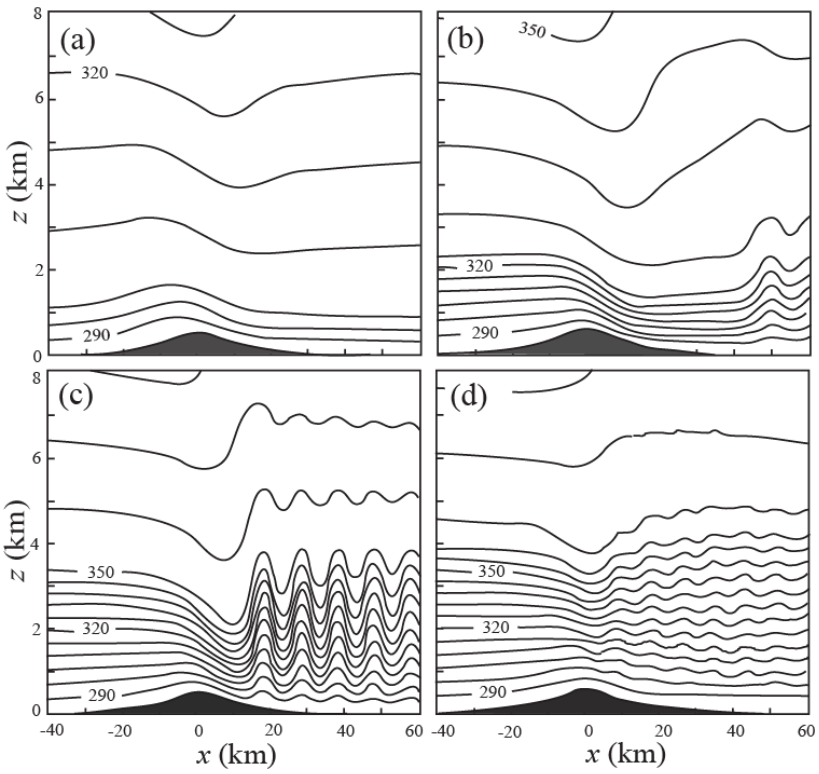

Fig. 5.16: The dependence of high-drag states on the lower-layer depth, as revealed by the isentropes for airflow in a two-layer atmosphere at $Ut/a = 25$, when $N_1 h/U = 0.5$, where N_1 is the Brunt-Vaisala frequency of the lower layer, and the depth of the lowest, most stable layer (U/N_1) is: (a) 1, (b) 2.5, (c) 3.5, and (d) 4. The lower layer resembles: (a) supercritical flow, (b) a propagating hydraulic jump, (c) a stationary jump, and (d) subcritical flow. (Lin 2007; After Durran 1986a)

The hydraulic theory of severe downslope winds was confirmed by numerical experiments of stratified fluid flow (e.g., Durran and Klemp 1987; Bacmeister and Pierrehumbert 1988) and laboratory tank experiments (e.g., Rottman and Smith 1989).

Note that in order to apply the hydraulic theory to the prediction of the steady-state flow over a mountain, it is necessary to specify the initial height of the dividing

streamline line. Thus, the dividing streamline height cannot be determined a priori if the critical level is induced by wave breaking.

This, in turn, implies that the hydraulic model is limited to the consistent check of a severe wind state and cannot be used for prediction (Wang and Lin 1999; Lin 2007).

- ***Discussion about Applications of resonant amplification and hydraulic theories*** (Wang and Lin 1999, Lin 2007)

Some discrepancies have been found between the resonant amplification and hydraulic theories of severe downslope windstorms.

One discrepancy is the different critical level heights for high-drag (severe wind) states predicted by these two theories. The resonant amplification theory predicts the wave-induced critical (wave breaking) level at a height of $z/\lambda_z = 3/4 + n$, where n is an integer, which helps produce severe downslope winds at later times.

On the other hand, the hydraulic theory predicts critical level heights falling within the range of $z/\lambda_z = 1/4 + n$ to $3/4 + n$ during a high-drag state. This discrepancy appears to be caused by different stages of the severe downslope wind state being used for prediction (Wang and Lin 1999; Lin 2007).

In fact, in earlier stages of a high-drag state, the resonant amplification theory is consistent with weakly nonlinear theories which indicate that the initiation of a high-drag transitional flow begins with linear resonance (Grimshaw and Smyth 1986), and with nonlinear numerical simulations which indicate that the lowest initial wave-induced critical level is near 3/4 (Lin and Wang 1996).

It can also be seen clearly from Fig. 5.10 that the wave-induced critical level for a severe-wind state is shifted to a lower level at later time. Therefore, it appears that the resonant amplification theory focuses on the earlier stage of severe downslope wind development, while the hydraulic theory focuses on the later stage.

Part of the discrepancies may be related to the usage of critical level height as the control parameter to determine a high-drag state, as often adopted in many previous studies. Based on some numerical experiments, the lower uniform flow layer depth appears to be a more appropriate scale to use (Wang and Lin 1999).

Figure 5.16 indicates that the high-drag state is sensitive to the lower stable layer depth (Durran 1986a). Using the lower layer depth as the control parameter, predictions of both high- and low-drag states from several previous numerical studies

are shown to be consistent, and the high-drag state does depend on the mountain height, which is consistent with the hydraulic theory (Wang and Lin 1999).

In addition, some discrepancies among previous studies result from the choice of different Richardson numbers and basic flow velocity profiles (e.g., Teixeira et al. 2005).

Appendix 5.1: Some mathematical techniques and relations

(a) Fourier Transform

The Fourier transform of $f(x)$ is defined as

$$\hat{f}(k) = \frac{1}{2\pi}\int_{-\infty}^{\infty} f(x)\, e^{-ikx} dx \text{ and} \qquad \text{(A5.1.1a)}$$

$$f(x) = \int_{-\infty}^{\infty} \hat{f}(k)\, e^{ikx} dk\,. \qquad \text{(A5.1.1b)}$$

One of the advantages of the Fourier transform is that it is able to distinguish the up- and down-going waves. An alternative Fourier transform pair may be defined as

$$\hat{f}(k) = \frac{1}{2\pi}\int_{-\infty}^{\infty} f(x)\, e^{-ikx} dx \text{ and} \qquad \text{(A5.1.2a)}$$

$$f(x) = 2\,\mathrm{Re}\int_{0}^{\infty} \hat{f}(k)\, e^{ikx} dk\,, \qquad \text{(A5.1.2b)}$$

for real function *f*. This is also called the *one-sided Fourier transform* (Queney et al. 1960). Occasionally, the following pair of Fourier transform has been adopted in the literature,

$$\hat{f}(k) = \frac{1}{\pi}\int_{-\infty}^{\infty} f(x)\, e^{-ikx} dx \text{ and} \qquad \text{(A5.1.3a)}$$

$$f(x) = \mathrm{Re}\int_{0}^{\infty} \hat{f}(k)\, e^{ikx} dk\,. \qquad \text{(A5.1.3b)}$$

Other variations of Fourier transform pairs, such as using e^{ikx} (e^{-ikx}) in the forward (inverse or backward) Fourier transform, have also been used in the literature. No matter which form of the Fourier transform is used, the Fourier transform pair should be able to transform the original function back to itself after performing the forward and inverse transforms.

(b) Jordan's Lemma

If

$$\lim_{R\to\infty}|f(z)|=0,$$

then

$$\lim_{R\to\infty}\int_{\Gamma_R} f(z)e^{ikz}dz=0, \tag{A5.1.4}$$

for $k>0$ and where Γ_R is an anticlockwise contour of a semicircle above the $\mathrm{Re}\,z$ axis with radius R. Jordan's Lemma is very useful for converting a line integral to a contour integral.

(c) Riemann-Lebesgue Lemma

$$\lim_{x\to\infty}\int_{-\infty}^{\infty}\hat{f}(k)e^{ikx}dk=0 \quad \text{if} \quad \hat{f}(k) \text{ is smooth.} \tag{A5.1.5}$$

A smooth function here means that the function is ordinary and absolutely integrable. The above conclusion is reached by the reasoning of cancellation.

(d) Parseval Theorem

$$\frac{1}{2\pi}\int_{-\infty}^{\infty}f(x)g^*(x)dx=\int_{-\infty}^{\infty}\hat{f}(k)\hat{g}^*(k)dk, \tag{A5.1.6}$$

where "^" indicates the Fourier transformed functions. The Parseval theorem is useful for computing wave energy and momentum flux.